

## Biosensors

How to cite: *Angew. Chem. Int. Ed.* **2023**, *62*, e202219024

International Edition: doi.org/10.1002/anie.202219024

German Edition: doi.org/10.1002/ange.202219024

# Functionalisation of Graphene Sensor Surfaces for the Specific Detection of Biomarkers

Laura von Lüders, Rita Tilmann, Kangho Lee, Cian Bartlam, Tanja Stimpel-Lindner, Tarja K. Nevanen, Kristiina Iljin, Kathrin C. Knirsch, Andreas Hirsch, and Georg S. Duesberg\*

**Abstract:** We report on a controllable and specific functionalisation route for graphene field-effect transistors (GFETs) for the recognition of small physiologically active molecules. Key element is the noncovalent functionalisation of the graphene surface with perylene bisimide (PBI) molecules directly on the growth substrate. This Functional Layer Transfer enables the homogeneous self-assembly of PBI molecules on graphene, onto which antibodies are subsequently immobilised. The sensor surface was characterised by atomic force microscopy, Raman spectroscopy and electrical measurements, showing superior performance over conventional functionalisation after transfer. Specific sensing of small molecules was realised by monitoring the electrical property changes of functionalised GFET devices upon the application of methamphetamine and cortisol. The concentration dependent electrical response of our sensors was determined down to a concentration of 300 ng ml<sup>-1</sup> for methamphetamine.

## Introduction

In recent years, the field of biosensor technology has advanced in response to the increased demand for detailed information on the health and physiological status of patients.<sup>[1]</sup> Up to now, there exists a range of biosensors working with human saliva, serum or tissues identifying chemical changes in the body, such as early indicators for diseases or stress and drug tests.<sup>[2]</sup> Conventional sensor technologies such as micro-nuclear magnetic resonance, surface plasmon resonance, mass spectrometry or immunofluorescence sensors demand either additional labelling or expensive instrumentation to analyse the data.<sup>[2-6]</sup> For mobile use and in-field application, portable and lightweight

sensors are required which produce quick results with the same excellent sensitivity and reliability.<sup>[1]</sup> Thus, a new and rapidly advancing field of research towards low-dimensional materials including carbon nanotubes, nanowires and graphene in biosensing has evolved in the past years.<sup>[7-12]</sup> Graphene sheets have been found to possess higher sensitivity, stability and signal-to-noise ratio than other evaluated materials.<sup>[12,13]</sup> Monolayer graphene features high electron mobility<sup>[14-18]</sup> and chemical stability in combination with a high surface area, making it an ideal transducer material for biological and chemical sensor applications.<sup>[19-22]</sup> Especially, graphene field-effect transistors (GFETs) have been proposed as ultra-high sensitive biosensors for mobile and point-of-care applications with real-time sensing.<sup>[7,23-25]</sup> Furthermore, the ambipolar behaviour of graphene allows for direct observation of n- or p-type doping due to molecule adsorption.<sup>[24,26,27]</sup> GFET biosensors have demonstrated excellent limit of detection and fast response time.<sup>[24,28]</sup> Moreover, it is advantageous to minimise the number of chemicals and processing steps in the fabrication as label-free sensors.<sup>[7,28]</sup>

One of the major challenges in 2D material-based sensors is the lack of selectivity towards specific target molecules, which is introduced by the functionalisation of the graphene surface. Various functionalisation routes have been investigated, including both covalent and noncovalent functionalisation strategies.<sup>[29-31]</sup> In the former, molecules bind to the graphene surface *via* the formation of sp<sup>3</sup>-bonds, often to the detriment of the electronic properties of the underlying 2D material.<sup>[6,28,32]</sup> In contrast to this, noncovalent functionalisation relies on interaction between molecules including van der Waals interaction,  $\pi$ - $\pi$ -stacking or electrostatic interaction.<sup>[33]</sup> This is more preferable as the graphene's intrinsic properties can be preserved,<sup>[25,30,34-37]</sup> as

[\*] L. von Lüders, R. Tilmann, Dr. K. Lee, Dr. C. Bartlam, Dr. T. Stimpel-Lindner, Prof. Dr. G. S. Duesberg  
Institute of Physics, EIT 2, Faculty of Electrical Engineering and Information Technology, University of the Bundeswehr Munich & SENS Research Center  
Werner-Heisenberg-Weg 39, 85 577 Neubiberg (Germany)  
E-mail: duesberg@unibw.de

Dr. T. K. Nevanen, Dr. K. Iljin  
VTT Technical Research Centre of Finland  
Tietotie 2, 02150 Espoo (Finland)

Dr. K. C. Knirsch, Prof. Dr. A. Hirsch  
Department of Chemistry and Pharmacy, Friedrich-Alexander-Universität (FAU) Erlangen-Nürnberg  
Nikolaus-Fiebiger-Straße 10, 91058 Erlangen (Germany)

© 2023 The Authors. Angewandte Chemie International Edition published by Wiley-VCH GmbH. This is an open access article under the terms of the Creative Commons Attribution Non-Commercial NoDerivs License, which permits use and distribution in any medium, provided the original work is properly cited, the use is non-commercial and no modifications or adaptations are made.

previously shown by using pyrene-based linkers.<sup>[38]</sup> However, both functionalisation routes are significantly influenced by the graphene quality and cleanliness.<sup>[39,40]</sup> Winters *et al.* have shown that perylene bisimide (PBI) self-assembled monolayers (SAMs) can be formed on graphene directly after its chemical vapour deposition (CVD) growth and transferred onto the target substrate using a polymer supporting layer on top of the PBI-graphene stack.<sup>[40]</sup> This transfer method, so-called Functional Layer Transfer (FLaT), has the advantage that the polymer layer is not in direct contact with graphene before functionalisation. As a result, it resembles a reliable starting point for following effective functionalisation by PBI SAM formation onto graphene.<sup>[40,41]</sup>

Additionally, antibody-antigen pairs can be used as recognition system for enhanced specificity of molecule detection.<sup>[42–45]</sup> Their unique binding mechanism towards one another is an excellent way to achieve a rapid and specific detection,<sup>[46]</sup> where either the antibody or the antigen is immobilised on a solid surface and the complementary molecule is introduced and detected.

In this study, we address both the selectivity and reproducibility issues facing graphene-based biosensors by noncovalent functionalisation with a perylene linker prior to wet-chemical transfer of as-grown CVD graphene. The carboxylic groups of the PBI are used to immobilise specific antibodies on the surface. Atomic force microscopy (AFM), Raman spectroscopy and electrical measurements show superior behaviour of FLaT graphene over conventional functionalisation. To further demonstrate the effectiveness of this functionalisation route, we choose two antibody-antigen pairs as example systems for highly specific sensing of small molecules: methamphetamine and cortisol. Methamphetamine is a stimulant drug affecting the central nervous system and abuse of this substance is of serious

concern in many regions worldwide.<sup>[47–51]</sup> Cortisol is a steroid hormone that is regulated by the central stress system of the human body and physiologically important.<sup>[1,52–54]</sup> Two electrical parameters (sheet resistance and Dirac voltage) are chosen to confirm the concentration dependency of the biosensor towards methamphetamine. They show responses at relevant concentration levels with sensitivities down to 300 ng ml<sup>-1</sup> for methamphetamine. The specificity of these biosensors is proven by testing alternative placebo molecules on the sensor platform where no cross-sensitivity can be observed.

## Results and Discussion

### Functional Layer Transfer

The graphene used in our experiments was grown *via* CVD on Cu foils. Scanning electron microscopy (SEM), Raman spectroscopy and AFM were performed and confirm the high quality of the graphene. The graphene domain size of 5–10 μm was determined using SEM (see Figure S4). The Raman signal of the conventionally transferred graphene on SiO<sub>2</sub>/Si substrate (Figure 1) shows the graphene 2D and G peaks at 2700 cm<sup>-1</sup> and 1582 cm<sup>-1</sup>, respectively, revealing monolayer graphene.<sup>[22,55,56]</sup> This is supported by the average full width at half maximum of the 2D peak of 35 cm<sup>-1</sup> (Figure S5a). The absence of the D peak at 1350 cm<sup>-1</sup> indicates a non-defective crystal structure.<sup>[56]</sup> This is supported by AFM analysis with a graphene monolayer height of 0.9 ± 0.2 nm (Figure 1d).<sup>[57,58]</sup> More details on the characterisation can be found in the Supporting Information.

We used the FLaT<sup>[40]</sup> to yield graphene layers with noncovalently attached PBI molecules, as can be seen in Figure 1a. For more details on the transfer procedures, see

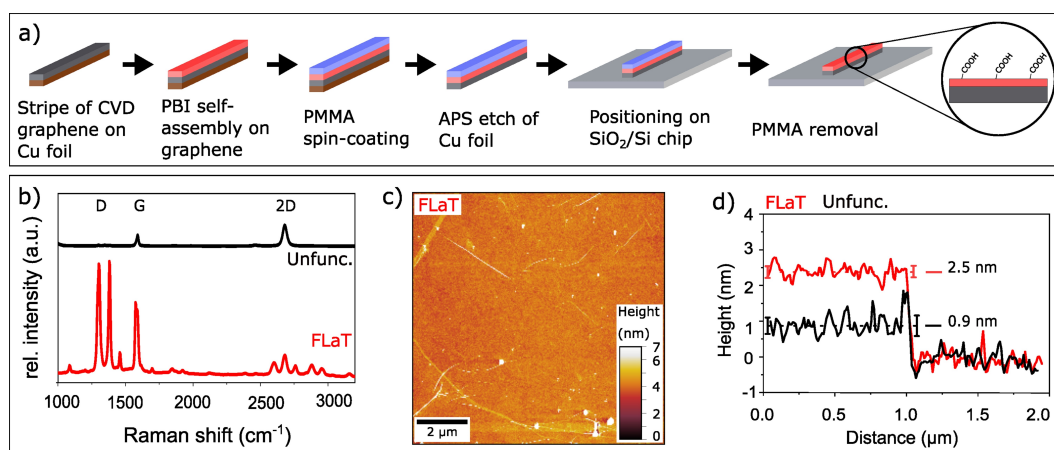


**Figure 1.** a) GFET fabrication schematics using the FLaT with PBI functionalisation directly after graphene growth and subsequent transfer (see Experimental Section). b) Average Raman spectra of unfunctionalised (black) and FLaT (red) graphene derived from the 100 × 100 μm<sup>2</sup> Raman maps depicted in Figure S5. The intensity ratio of 2D and G peaks indicates monolayer graphene. The intense perylene peaks at 1301 cm<sup>-1</sup> and 1381 cm<sup>-1</sup><sup>[6]</sup> demonstrate successful PBI functionalisation. c) AFM image of FLaT graphene showing smooth graphene and little surface contamination. d) Height profiles across an edge of graphene to substrate. Unfunctionalised graphene (black) has a height of 0.9 nm associated with monolayer graphene while FLaT graphene (red) shows a height of 2.5 nm, which indicates a PBI monolayer with a layer height of 1.6 nm. Respective AFM scans are shown in Figure S6.

the Experimental Section (Supporting Information). The PBI functionalised graphene shows prominent Raman peaks attributed to PBI at  $1301\text{ cm}^{-1}$  and  $1381\text{ cm}^{-1}$ <sup>[6]</sup> and homogeneous coverage in the Raman map in Figure S5c. The high intensity of these two peaks indicates successful functionalisation of the graphene with a high packing density of the PBI molecules.

As previously published, the FLaT process yields clean and homogeneous surfaces with defined carboxylic functions.<sup>[40]</sup> This can be seen in the AFM image in Figure 1c, which displays a  $10 \times 10\ \mu\text{m}^2$  topographic AFM scan of the FLaT graphene. The surface roughness ( $S_a$ ) of FLaT graphene is with  $0.44\text{ nm}$  much lower than the  $0.99\text{ nm}$  of unfunctionalised graphene (Figure S6a). In comparison to the conventional method of PBI functionalisation after PMMA based transfer, which possesses a surface roughness of  $0.85\text{ nm}$  (Figure S6b), the FLaT route yields smoother and more homogeneous surfaces. The height profiles (Figure 1d, profiles taken from Figure S6d and f) reveal a FLaT layer height of  $2.5 \pm 0.2\text{ nm}$ . This corresponds to an approximately  $1.6\text{ nm}$  thick PBI film on top of monolayer graphene. Tilmann *et al.* and Wirtz *et al.* have used similar perylene molecules with slightly smaller side chains and observed molecule layer heights of roughly  $1\text{ nm}$  and  $1.2\text{ nm}$ , respectively.<sup>[6,32]</sup>

### Biosensor development

The FLaT graphene was further functionalised with antibodies to produce the GFET biosensor platform (see Figure 2). The amine groups of monoclonal methamphetamine-AB were coupled to the carboxylic groups of the PBI

via EDC/NHS coupling (for details see Experimental Section (Supporting Information)), allowing for the antibodies to bind specifically to the sensor (Figure 2c).<sup>[52,54,59]</sup> Subsequently, methamphetamine was introduced, which binds to the active site of the methamphetamine-AB. To assess the surface changes upon the molecule binding, AFM measurements were carried out. The AFM profile, indicated by the dashed blue line in Figure 2e, reveals a sample height of  $7.6 \pm 0.2\text{ nm}$ . Considering the previously discussed FLaT graphene height of  $2.5 \pm 0.2\text{ nm}$ , the antibody height calculates to approximately  $5.1\text{ nm}$ . In comparison to the methamphetamine-AB, the size of the small analyte methamphetamine (see Supporting Information) is negligible. The measured height fits with the assumption of randomly positioned antibodies that are not commonly standing in upright position.<sup>[43,60]</sup> Amine groups are distributed over the whole antibody, which results in a random immobilisation of the antibody onto the PBI surface. Possible antibody orientations include vertical alignment of methamphetamine-AB active sites (Y-shape) and horizontal alignment to the substrate with either one or no active site vertically aligned.<sup>[42,45,60]</sup> In summary, a homogeneously distributed monolayer of methamphetamine-ABs was found to cover the FLaT graphene surface. This indicates that the specific coupling of the methamphetamine-ABs to the PBI via amine coupling was achieved.

We use the same procedure to functionalise the FLaT graphene with cortisol binding Fab-fragments, which is the part of an antibody that includes the active site for antigen binding, and subsequently cortisol small molecules (see Figure S2).

### Electrical Characterisation of Biosensors

The electrical performance of 191 individual GFETs with respect to various treatments was examined and is displayed in Figure 3.

Since the initial performance of individual GFETs differs considerably from each other (see Figure S7), we use the relative changes of sheet resistance ( $\Delta R_s$ ) and Dirac voltage ( $\Delta V_{\text{Dirac}}$ ) of each GFET to extract actual variance driven by chemical treatment. Therefore, one data point consists of two measurements of the same GFET, one before and one after treatment so that the actual change of electrical performance is derived. The results of the electrical characterisation of all GFETs with the same functionalisation were averaged and plotted as one column each (Figure 3a–d). For more details on the calculations, see Supporting Information.

In Figure S8, FLaT and conventionally functionalised GFETs were modified with methamphetamine-AB and were directly compared upon exposure to  $10\ \mu\text{gml}^{-1}$  methamphetamine solution. The overall change of conventionally functionalised GFETs is less ( $\approx 30\%$ ) than the FLaT GFETs ( $\approx 60\%$ ) in most devices, particularly with respect to  $\Delta V_{\text{Dirac}}$ , where the response for FLaT is almost 4 times as strong. Also, the standard deviations for the  $\Delta R_s$  of the

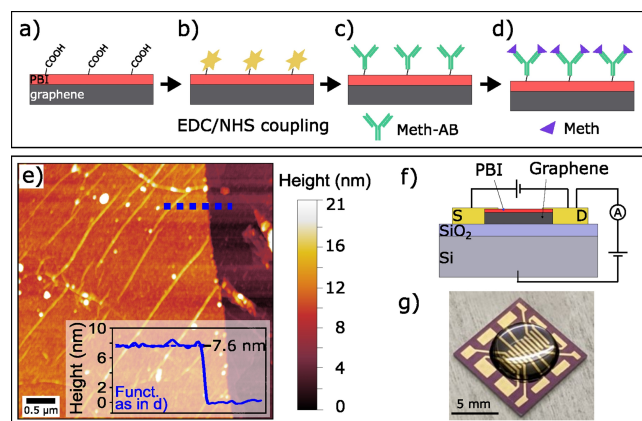


**Figure 2.** Process flow of GFET methamphetamine biosensor fabrication and sensor test. a) FLaT graphene transferred onto  $\text{SiO}_2/\text{Si}$ . b) On-chip activation of the carboxylic groups of the PBI using EDC/NHS coupling. c) Amine-coupling of the PBI to methamphetamine-AB. d) Methamphetamine attachment. e) AFM image of a fully functionalised methamphetamine biosensor as in Figure 2d. Scan area of  $4.5 \times 4.5\ \mu\text{m}^2$  with a blue dashed line indicating the height profile displayed in the inset. The sample height of  $7.6\text{ nm}$  reveals a  $5.1\text{ nm}$  thick methamphetamine-AB monolayer on top of FLaT graphene. f) Schematic cross-section of GFET and g) photograph of GFET with analyte solution.

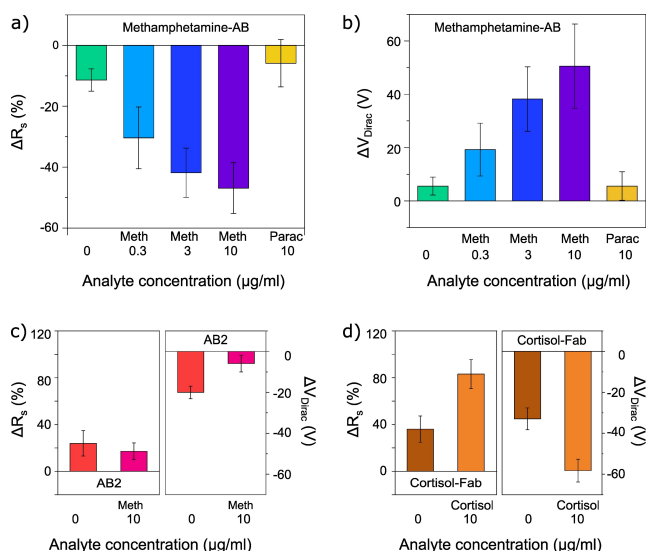


**Figure 3.** Averaged electrical measurements of GFETs for the detection of methamphetamine and cortisol. a)  $\Delta R_s$  and b)  $\Delta V_{\text{Dirac}}$  after methamphetamine-AB coupling and analyte exposure: No analyte (green), exposure to 0.3, 3 and 10  $\mu\text{g ml}^{-1}$  (light blue, dark blue and purple, respectively) of methamphetamine, exposure to 10  $\mu\text{g ml}^{-1}$  of paracetamol (yellow). Specific detection of methamphetamine in various concentrations with no cross-sensitivity to paracetamol is revealed. Number of measured devices from left to right: 24, 29, 32, 26, 12. c)  $\Delta R_s$  and  $\Delta V_{\text{Dirac}}$  for control measurements with AB2 (red) coupling to the PBI and additional 10  $\mu\text{g ml}^{-1}$  methamphetamine (pink) exposure, indicating some unspecific adsorption of methamphetamine. Number of measured devices from left to right: 10, 23. d)  $\Delta R_s$  and  $\Delta V_{\text{Dirac}}$  of cortisol-Fab (brown) coupled to the PBI and after cortisol (orange) exposure, revealing a strong response due to the specific analyte binding. Number of measured devices from left to right: 18, 17. Details on values and error bars can be found in Table S1 and Table S2 in the Supporting Information.

conventionally functionalised samples are much larger in FLAT GFETs.

Due to the superior performance, we further investigated FLAT derived GFETs in terms of their specific and concentration dependent response. The green column in Figure 3a and b represent  $\Delta R_s$  and  $\Delta V_{\text{Dirac}}$  for methamphetamine-AB coupled GFETs without exposure to any analyte, which results in only slight changes in the electrical performance compared to the initial state. When GFETs were exposed to 0.3, 3 or 10  $\mu\text{g ml}^{-1}$  methamphetamine solution, a clear concentration dependent relation between the concentration and  $\Delta R_s$  or  $\Delta V_{\text{Dirac}}$  was observed. Specifically, the  $\Delta R_s$  decreased from  $-11\%$  to  $-47\%$  across the concentration range from 0 to 10  $\mu\text{g ml}^{-1}$  methamphetamine (Table S1). Equivalently, the  $\Delta V_{\text{Dirac}}$  increased from 6 V to 51 V in the same range (Table S2). These distinct concentration dependent responses in both  $\Delta R_s$  and  $\Delta V_{\text{Dirac}}$  demonstrate the successful detection of methamphetamine by the biosensor. The limit of detection has not been met using the lowest methamphetamine concentration applied here.

To assess the selectivity of the sensor, cross detection with paracetamol was carried out. This molecule was chosen as a non-specific control due to its similar size compared to

methamphetamine (see Supporting Information). The addition of 10  $\mu\text{g ml}^{-1}$  paracetamol onto the GFETs after methamphetamine-AB coupling does not alter the electrical parameters and shows similar results as without analyte application, which can be seen for both  $\Delta R_s$  and  $\Delta V_{\text{Dirac}}$ . This result verifies the specificity of the methamphetamine biosensors towards the explicit detection of methamphetamine through methamphetamine-AB.

All GFETs commonly show a positive shift of the  $V_{\text{Dirac}}$  after the respective treatments, indicating p-type doping. Graphene is naturally p-doped in ambient conditions and remains sensitive to major charge carrier density changes, which results in the observed  $\Delta R_s$  decrease and  $V_{\text{Dirac}}$  increase.<sup>[61]</sup>

Further control measurements were performed: Instead of methamphetamine-AB, the AB2 as a nonspecific antibody was coupled to the PBI of the FLAT graphene. In Figure 3c, the  $\Delta R_s$  and  $\Delta V_{\text{Dirac}}$  of GFETs after AB2 coupling and subsequent methamphetamine application are displayed. The addition of methamphetamine onto AB2 does not show any notable changes in  $\Delta R_s$ , but the  $\Delta V_{\text{Dirac}}$  is decreased by 14 V. This may indicate that a certain amount of methamphetamine molecules non-specifically adsorbs onto the AB2 functionalised FLAT graphene. This is a common issue in graphene sensing that has been stated in previous reports.<sup>[19,23,37,62]</sup> Nevertheless, the impact of methamphetamine onto the non-specific AB2 is small, compared to the specific methamphetamine-AB, which results in an increase in  $\Delta V_{\text{Dirac}}$  of one order of magnitude.

The second antibody-antigen system was chosen to demonstrate the versatility of the FLAT derived biosensors; thus, a cortisol Fab-fragment (cortisol-Fab) was coupled to the PBI on the FLAT GFETs via amine-coupling. The  $\Delta R_s$  and  $\Delta V_{\text{Dirac}}$  after exposure to the cortisol solution are displayed in Figure 3d. The strong  $\Delta R_s$  increase and  $\Delta V_{\text{Dirac}}$  decrease show the high sensitivity towards cortisol. The direction of the shift indicates n-type doping behaviour due to the presence of cortisol as is in agreement with previous reports.<sup>[53,63]</sup> This supports the previously discussed antibody-antigen coupling mechanism being a versatile way of functionalisation of graphene for biosensing applications.

## Conclusion

The noncovalent functionalisation of graphene with PBI molecules via the FLAT route was demonstrated to be a viable approach for label-free sensing of small biomarker molecules. The high specificity of the GFETs is based on the binding principles of (1) the PBI molecule acting as the linker towards antibodies via amine-coupling and, (2) the unique interaction of the antibody to the methamphetamine via the specific antibody-antigen binding. Both principles were verified by AFM and electrical measurements. A concentration dependent response towards different methamphetamine concentrations was revealed. Control measurements have demonstrated that the small molecule paracetamol does not bind to the sensor platform, implying no cross-reactivity of the methamphetamine biosensor to a

placebo of similar size. Additionally, electrical measurements with a second antibody-antigen system—cortisol—promise a general applicability of the method. The specific and concentration dependent sensing of small molecules on PBI-functionalised graphene represents a major step for versatile sensors, which can be extended to other antibody-antigen systems.

In future work, we will standardise the preparation and functionalisation processes for deeper insight into the limit of detection of methamphetamine biosensors and apply the principle to further antibody-antigen pairs.

### Acknowledgements

This project has received funding from the European Union's Horizon 2020 research and innovation program under grant agreement No. 881603 (Graphene Flagship Core 3). Further, this project was supported with funds from the German Federal Ministry for Education and Research (BMBF) for projects ACDC 13N15100. We thank detec.bw—Digitalization and Technology Research Center of the Bundeswehr for support [project VITAL-SENSE]. detec.bw is funded by the European Union—NextGenerationEU. Special thanks to Oliver Hartwig for providing the schematic image of a functionalised graphene field-effect transistor displayed in the graphical abstract. Open Access funding enabled and organized by Projekt DEAL.

### Conflict of Interest

The authors declare no conflict of interest.

### Data Availability Statement

The data that support the findings of this study are available from the corresponding author upon reasonable request.

**Keywords:** Antibody-Antigen System • Biosensors • Functional Layer Transfer • Graphene • Noncovalent Functionalization

- [1] O. Parlak, S. T. Keene, A. Marais, V. F. Curto, P. Samori, *Sci. Adv.* **2018**, *4*, 7.
- [2] D. Kwong Hong Tsang, T. J. Lieberthal, C. Watts, I. E. Dunlop, S. Ramadan, *Sci. Rep.* **2019**, *9*, 13946.
- [3] R. Vaidyanathan, M. Naghibosadat, S. Rauf, D. Korbie, L. G. Carrascosa, *Anal. Chem.* **2014**, *86*, 11125–11132.
- [4] H. Im, H. Shao, Y. I. Park, V. M. Peterson, C. M. Castro, *Nat. Biotechnol.* **2014**, *32*, 490–495.
- [5] S. S. Kanwar, C. J. Dunlay, D. M. Simeone, S. Nagrath, *Lab Chip* **2014**, *14*, 1891–1900.
- [6] R. Tilmann, C. Weiß, C. P. Cullen, L. Peters, O. Hartwig, *Adv. Electron. Mater.* **2021**, *7*, 2000564.
- [7] N. Gao, T. Gao, X. Yang, X. Dai, W. Zhou, *Proc. Natl. Acad. Sci. USA* **2016**, *113*, 14633–14638.
- [8] A. Zhang, C. M. Lieber, *Chem. Rev.* **2016**, *116*, 215–257.

- [9] N. G. Shang, P. Papakonstantinou, M. McMullan, M. Chu, A. Stamboulis, *Adv. Funct. Mater.* **2008**, *18*, 3506–3514.
- [10] J.-F. Wu, M.-Q. Xu, G.-C. Zhao, *Electrochem. Commun.* **2010**, *12*, 175–177.
- [11] V. Vamvakaki, K. Tsagaraki, N. Chaniotakis, *Anal. Chem.* **2006**, *78*, 5538–5542.
- [12] M. Pumera, A. Ambrosi, A. Bonanni, E. L. K. Chng, H. L. Poh, *TrAC Trends Anal. Chem.* **2010**, *29*, 954–965.
- [13] S. Alwarappan, A. Erdem, C. Liu, C.-Z. Li, *J. Phys. Chem. C* **2009**, *113*, 8853–8857.
- [14] W. Zhu, H. Shi, W. Gan, P. Li, C. Wu, *Mater. Res. Express* **2018**, *5*, 075005.
- [15] S. Xu, T. Wang, G. Liu, Z. Cao, L. A. Frank, *Sens. Actuators B* **2021**, *326*, 128991.
- [16] M. C. Lemme, T. J. Echtermeyer, M. Baus, H. Kurz, *IEEE Electron Device Lett.* **2007**, *28*, 282–284.
- [17] F. Xia, D. B. Farmer, Y. Lin, P. Avouris, *Nano Lett.* **2010**, *10*, 715–718.
- [18] M. Y. Han, B. Ozyilmaz, Y. Zhang, P. Kim, *Phys. Rev. Lett.* **2007**, *98*, 206805.
- [19] Y. Liu, X. Dong, P. Chen, *Chem. Soc. Rev.* **2012**, *41*, 2283–2307.
- [20] F. Schedin, E. Lidorikis, A. Lombardo, V. G. Kravets, A. K. Geim, *J. Mol. Struct.* **2010**, *1040*, 213–215.
- [21] Y. Huang, X. Dong, Y. Shi, C. M. Li, L.-J. Li, P. Chen, *Nanoscale* **2010**, *2*, 1485–1488.
- [22] S. Winters, *PhD thesis*, Trinity College Dublin (Ireland), **2015**.
- [23] I. Novodchuk, M. Bajcsy, M. Yavuz, *Carbon* **2021**, *172*, 431–453.
- [24] S. Wang, M. Z. Hossain, T. Han, K. Shinozuka, T. Suzuki, *ACS Omega* **2020**, *5*, 30037–30046.
- [25] Z. Jiang, B. Feng, J. Xu, T. Qing, P. Zhang, *Biosens. Bioelectron.* **2020**, *166*, 112471.
- [26] P. R. Wallace, *Phys. Rev.* **1947**, *71*, 622–634.
- [27] J.-C. Charlier, P. C. Eklund, J. Zhu, A. C. Ferrari, *Top. Appl. Phys.* **2008**, *111*, 673–709.
- [28] C. Anichini, W. Czepa, D. Pakulski, A. Aliprandi, A. Ciesielski, *Chem. Soc. Rev.* **2018**, *47*, 4860–4908.
- [29] T. S. Sreeprasad, V. Berry, *Small* **2013**, *9*, 341–350.
- [30] M. Dieng, M. Bensifia, J. Borme, I. Florea, C. M. Abreu, *J. Phys. Chem. C* **2022**, *126*, 4522–4533.
- [31] H. Y. Mao, Y. H. Lu, J. D. Lin, S. Zhong, A. T. S. Wee, *Prog. Surf. Sci.* **2013**, *88*, 132–159.
- [32] C. Wirtz, T. Hallam, C. P. Cullen, N. C. Berner, M. O'Brien, *Chem. Commun.* **2015**, *51*, 16553–16556.
- [33] J. Liu, J. Tang, J. J. Gooding, *J. Mater. Chem.* **2012**, *22*, 12435–12452.
- [34] Z. Zhang, H. Huang, X. Yang, L. Zang, *J. Phys. Chem. Lett.* **2011**, *2*, 2897–2905.
- [35] Z. Meng, R. M. Stolz, L. Mendecki, K. A. Mirica, *Chem. Rev.* **2019**, *119*, 478–598.
- [36] Y. Ohno, K. Maehashi, K. Matsumoto, *J. Am. Chem. Soc.* **2010**, *132*, 18012–18013.
- [37] J. A. Mann, T. Alava, H. G. Craighead, W. R. Dichtel, *Angew. Chem. Int. Ed.* **2013**, *52*, 3177–3180.
- [38] M. Singh, M. Holzinger, M. Tabrizian, S. Winters, N. C. Berner, *J. Am. Chem. Soc.* **2015**, *137*, 2800–2803.
- [39] N. C. Berner, S. Winters, C. Backes, C. Yim, K. C. Dumbgen, *Nanoscale* **2015**, *7*, 16337–16342.
- [40] S. Winters, N. C. Berner, R. Mishra, K. C. Dumbgen, C. Backes, *Chem. Commun.* **2015**, *51*, 16778–16781.
- [41] H. Kim, W. Kim, M. O'Brien, N. McEvoy, C. Yim, *Nanoscale* **2018**, *10*, 17557–17566.
- [42] J. Baniukevic, J. Kirlyte, A. Ramanavicius, A. Ramanaviciene, *Sens. Actuators B* **2013**, *189*, 217–223.
- [43] N. G. Welch, J. A. Scoble, B. W. Muir, P. J. Pigram, *Biointerphases* **2017**, *12*, 02D301.

- [44] C. Qi, J.-Z. Duan, Z.-H. Wang, Y.-Y. Chen, P.-H. Zhang, *Biomed. Microdevices* **2006**, *8*, 247–253.
- [45] J. G. Vilhena, A. C. Dumitru, E. T. Herruzo, J. I. Mendieta-Moreno, R. Garcia, *Nanoscale* **2016**, *8*, 13463–13475.
- [46] J. Zorea, R. P. Shukla, M. Elkabets, H. Ben-Yoav, *Anal. Bioanal. Chem.* **2020**, *412*, 1709–1717.
- [47] E. C. Peterson, W. B. Gentry, S. M. Owens, *Adv. Pharmacol.* **2014**, *69*, 107–127.
- [48] A. K. Cho, *Science* **1990**, *249*, 631–634.
- [49] European Monitoring Centre for Drugs and Drug Addiction, “Health and social Responses for methamphetamine users”, can be found under <https://www.emcdda.europa.eu/>, **2014**.
- [50] R. A. Rawson, R. Gonzales, P. Brethen, *J. Subst. Abuse. Treat.* **2002**, *23*, 145–150.
- [51] J. Mendelson, N. Uemura, D. Harris, R. P. Nath, E. Fernandez, *Clin. Pharmacol. Ther.* **2006**, *80*, 403–420.
- [52] K. Sun, N. Ramgir, S. Bhansali, *Sens. Actuators B* **2008**, *133*, 533–537.
- [53] M. Ku, J. Kim, J.-E. Won, W. Kang, Y.-G. Park, *Sci. Adv.* **2020**, *6*, eabb2891.
- [54] R. M. Torrente-Rodríguez, J. Tu, Y. Yang, J. Min, M. Wang, *Matter* **2020**, *2*, 921–937.
- [55] A. C. Ferrari, D. M. Basko, *Nat. Nanotechnol.* **2013**, *8*, 235–246.
- [56] L. Bao, B. Zhao, V. Lloret, M. Halik, F. Hauke, *Angew. Chem. Int. Ed.* **2020**, *59*, 6700–6705.
- [57] A. Sidorenko, T. Krupenkin, A. Taylor, P. Fratzl, J. Aizenberg, *Science* **2007**, *315*, 487–490.
- [58] F. Qing, Y. Zhang, Y. Niu, R. Stehle, Y. Chen, *Nanoscale* **2020**, *12*, 10890–10911.
- [59] J. Kudr, L. Zhao, E. P. Nguyen, H. Arola, T. K. Nevanen, *Biosens. Bioelectron.* **2020**, *156*, 112109.
- [60] Y. Sun, H. Du, C. Feng, Y. Lan, *J. Solid State Electrochem.* **2015**, *19*, 3035–3043.
- [61] S. Goniszewski, M. Adabi, O. Shaforost, S. M. Hanham, L. Hao, *Sci. Rep.* **2016**, *6*, 22858.
- [62] F. Wu, P. A. Thomas, V. G. Kravets, H. O. Arola, M. Soikkeli, *Sci. Rep.* **2019**, *9*, 20286.
- [63] N. N. M. Maidin, R. A. Rahim, N. H. A. Halim, A. S. Z. Abidin, N. A. Ahmad, *AIP Conference Proceedings*, **2018**, p. 20022.

Manuscript received: December 23, 2022

Accepted manuscript online: March 19, 2023

Version of record online: April 25, 2023